Earth and Planetary Science Letters 393 (2014) 120–131

Contents lists available at ScienceDirect

Earth and Planetary Science Letters

www.elsevier.com/locate/epsl

Reconstructing the deep CO_2 degassing behaviour of large basaltic fissure eruptions

Margaret E. Hartley [a,*], John Maclennan [a], Marie Edmonds [a], Thor Thordarson [b,c]

[a] Department of Earth Sciences, University of Cambridge, Downing Street, Cambridge, CB2 3EQ, UK
[b] School of GeoSciences, University of Edinburgh, Grant Institute, West Mains Road, Edinburgh, EH9 3JW, UK
[c] Institute of Earth Sciences, University of Iceland, Sturlugata 7, 101 Reykjavík, Iceland

ARTICLE INFO

Article history:
Received 5 November 2013
Received in revised form 6 February 2014
Accepted 12 February 2014
Available online 15 March 2014
Editor: B. Marty

Keywords:
melt inclusion
shrinkage bubble
Raman spectroscopy
carbon dioxide
degassing

ABSTRACT

The mass of volatiles degassed from volcanic eruptions is often estimated by comparing the volatile concentrations in undegassed glassy melt inclusions with the volatile concentrations in the degassed matrix glass. However, melt inclusions are prone to post-entrapment modification, including diffusive H^+ loss through the host olivine crystal lattice which lowers the H_2O content of the inclusion, and the degassing of CO_2 into a bubble in response to cooling and crystallisation on the inclusion walls. Such bubbles are very common in olivine-hosted melt inclusions from the AD 1783–1784 Laki eruption, south-east Iceland. We have determined the CO_2 content of these bubbles using micro-Raman spectroscopy, and the CO_2 concentration in the glass by SIMS. Our results show that >90% of the total inclusion CO_2 may be sequestered into the bubble, which demonstrates the importance of measuring the compositions of both vapour bubbles and the glass phase in melt inclusions. We reconstruct the deep degassing path of the Laki magma by using Nb as proxy for the undegassed CO_2 content of the melt inclusions. The substantial CO_2/Nb variation in the Laki melt inclusions (3.8–364) can be explained by concurrent crystallisation and CO_2 degassing in the Laki magmatic system. We calculate the amount of CO_2 lost from individual melt inclusions, assuming CO_2/Nb $\approx$ 435 for enriched Icelandic mantle and CO_2/Nb $\approx$ 171 for depleted mantle. Melt inclusions with the greatest saturation pressures have lost the least CO_2 prior to inclusion trapping. At any given saturation pressure, the most enriched melt inclusions have lost the most CO_2, while the most depleted inclusions have lost very little CO_2. Enriched primary melts with high initial CO_2 concentrations are therefore useful for investigating deep degassing behaviour in magmatic systems because a range of melt inclusion saturation pressures are recorded during crystallisation and degassing. Depleted melt inclusions with low initial CO_2 concentrations remain vapour-undersaturated to shallow levels and cannot be used to constrain deep degassing behaviour. The cumulative CO_2 mass release from the Laki magma is determined as a function of pressure and extent of crystallisation. Using an updated petrologic method that takes into account the diversity of primary melts and CO_2 sequestration into vapour bubbles, we calculate the total mass of CO_2 exsolved from the Laki magma to be 304 Mt.

1. Introduction

The total atmospheric yield of volatile species from volcanic eruptions is often estimated using a petrologic approach, comparing volatile concentrations measured in crystal-hosted melt inclusions with glass from quenched eruption products (e.g. Devine et al., 1984; Sigurdsson et al., 1985; Palais and Sigurdsson, 1989; Sigurdsson, 1990; Métrich et al., 1991; Thordarson et al., 1996). Such calculations rely on the assumption that the melt inclusions with the highest volatile concentrations are representative of pristine, undegassed melts. This assumption is reasonable for soluble volatile species such as water, sulphur, chlorine and fluorine, which may remain largely dissolved in basaltic magmas to shallow crustal depths (e.g. Schilling et al., 1980; Wallace and Carmichael, 1992; Carroll and Webster, 1994; Webster et al., 1999; Dixon et al., 1995). However, carbon dioxide has limited solubility in basaltic melts, and depending on the initial CO_2 concentration, basaltic liquids may become saturated with a CO_2-rich vapour at depths of 25 km or more (e.g. Pan et al., 1991; Dixon, 1997; Papale, 1999; Shishkina et al., 2010), such that melt inclusions trapped at mid-crustal depths usually do not preserve the initial CO_2 content of the magma (e.g. Fischer and Marty, 2005). This means that, while CO_2 concentrations in melt inclusions can be used to assess the 'erupted' CO_2 budget associated with melt ascent from the magma chamber to the surface, the petrologic method will underestimate

* Corresponding author.
E-mail address: meh43@cam.ac.uk (M.E. Hartley).

http://dx.doi.org/10.1016/j.epsl.2014.02.031
0012-821X

the total mass of CO_2 degassed from primary mantle melts supplied to the magmatic system and cannot be used to estimate the degree of passive CO_2 release in the lower crust.

1.1. Estimating undegassed volatile concentrations in melt inclusions

Volatile-trace element pairs, such as CO_2 and Nb or H_2O and Ce, have similar partition coefficients in basaltic melts and are expected to exhibit similar geochemical behaviour during the crystallisation of volatile-undersaturated melts (e.g. Michael, 1995; Danyushevsky et al., 2000b; Dixon and Clague, 2001; Saal et al., 2002; Michael and Graham, 2013). This indicates that Nb can be used as a proxy for the undegassed CO_2 content of melts, if the CO_2/Nb of the primary melt is known. This ratio can be estimated from volatile and trace element concentrations measured in rare examples of undegassed melt inclusions, which are expected to exhibit strong positive correlations between volatile species and similarly incompatible trace elements. Such correlations have been reported for CO_2 and Nb for a suite of primitive melt inclusions from the Siqueiros transform fault on the East Pacific Rise (Saal et al., 2002), and were interpreted as evidence that the melt was vapour-undersaturated at the time of inclusion trapping (Saal et al., 2002). Various studies have used CO_2/Nb, H_2O/Ce and other volatile/trace element ratios to estimate magmatic volatile fluxes (Saal et al., 2002; Workman et al., 2006; Cartigny et al., 2008; Koleszar et al., 2009; Shaw et al., 2010; Helo et al., 2011). However, carbon is likely to be heterogeneously distributed in the mantle (e.g. Helo et al., 2011), meaning that the CO_2/Nb estimated for undegassed primary melts varies with location. At the lower end of the global range, the highly depleted Siqueiros melt inclusions record $CO_2/Nb = 239 \pm 46$. At the upper end of the global range, CO_2/Nb values of ~570 have been obtained for MORB glass samples dredged around 14 °N and 34 °N along the Mid-Atlantic Ridge (Cartigny et al., 2008), and CO_2/Nb values of 650–800 have been reported in melt inclusions from Axial seamount, Juan de Fuca Ridge (Helo et al., 2011). The only reported undegassed CO_2/Nb value for Iceland, 314 ± 125, was determined using melt inclusions from the Borgarhraun lava, North Iceland (Hauri et al., 2002). The global variability in CO_2/Nb for undegassed primary melts suggests that CO_2 is slightly more incompatible than Nb during mantle melting. It has recently been suggested that CO_2 has similar geochemical behaviour to Ba or Rb, and CO_2/Ba values of 114 ± 43 have recently been reported for MORB compositions ranging from ultra-depleted to highly enriched (Michael and Graham, 2013). This may indicate that Ba is a better proxy for undegassed CO_2 than Nb, especially since Ba is expected to follow CO_2 more closely during subduction and recycling into the deep mantle (Michael and Graham, 2013).

1.2. Bubble formation in melt inclusions

Volatiles in melt inclusions can be affected strongly by post-entrapment modification and re-equilibration (e.g. Nielsen et al., 1998; Danyushevsky et al., 2000a; Steele-MacInnis et al., 2011; Gaetani et al., 2012). Bubbles in melt inclusions can form in a number of distinct stages. Firstly, shrinkage bubbles form in response to cooling, since the host phenocryst undergoes significantly less thermal contraction than the melt phase (e.g. Roedder, 1979; Lowenstern, 1995, 2003; Schiano, 2003; Métrich and Wallace, 2008). If the melt inclusion is volatile-free, the bubble will be almost a vacuum (Steele-MacInnis et al., 2011). For volatile-bearing melt inclusions, some of the volatiles that were originally dissolved in the silicate melt may exsolve and be sequestered into the bubble (e.g. Roedder, 1979; Skirius et al., 1990; Anderson and Brown, 1993; Cervantes et al., 2002). Bubbles formed by this mechanism are most likely to be formed at the Earth's surface, during the cooling of erupted magmas. Secondly, bubble growth occurs during post-entrapment crystallisation (PEC) on the melt inclusion walls. This process decreases the internal pressure of the inclusion, which lowers the solubility of volatiles in the melt phase and causes volatile exsolution from the melt (Steele-MacInnis et al., 2011). Thirdly, recent experimental studies have demonstrated that rapid H^+ diffusion can cause olivine-hosted melt inclusions to re-equilibrate with their carrier liquids within tens of hours at magmatic temperatures of ~1200° (Gaetani et al., 2012; Bucholz et al., 2013). Decompression associated with diffusive H^+ loss may promote further volatile exsolution, leading to the nucleation of a vapour bubble in a previously bubble-free inclusion, or the growth of a pre-existing bubble. Since CO_2 is relatively insoluble in basaltic melts in comparison to other common volatile species, CO_2 vapour will be preferentially sequestered into the bubble if post-entrapment degassing occurs. The role of shrinkage bubbles in controlling the volatile content of melt inclusions has been largely avoided or ignored in the literature, although there are some notable exceptions (e.g. Kamenetsky et al., 2002; Thomas et al., 2006; Métrich and Wallace, 2008; Hansteen and Klügel, 2008).

1.3. The AD 1783–1784 Laki eruption

The AD 1783–1784 Laki (Skaftár Fires) fissure eruption on Iceland's Eastern Volcanic Zone was one of the largest basaltic fissure eruptions recorded in human history (e.g. Thordarson et al., 2003), and is one of the best-studied small-scale analogues of a flood basalt eruption. The eruption produced 14.7 km^3 of lava and ~0.4 km^3 dense rock equivalent of tephra from a ~27 km-long fissure that erupted sequentially in 10 en echelon segments (Thordarson and Self, 1993). The eruption was one of the greatest natural atmospheric pollution events of the past ~250 years, loading the atmosphere with 122 Mt sulphur dioxide, ~7.0 Mt hydrochloric acid and ~15.0 Mt hydrofluoric acid in a period of 8 months (Thordarson et al., 1996) and leading to significant climatic effects that were felt across the northern hemisphere (e.g. Thordarson and Self, 2003; Chenet et al., 2005; Oman et al., 2006; Schmidt et al., 2010, 2012).

The presence of vapour bubbles in Laki melt inclusions has been noted in previous studies (e.g. Métrich et al., 1991; Thordarson et al., 1996), making the Laki eruption an ideal case study for investigating the effect of bubble formation on melt inclusion volatile systematics. We present the first study to combine measurements of vapour compositions in these bubbles with volatile concentrations in the glass phase, in order to determine the total volatile content of melt inclusions at the time of inclusion trapping. We use CO_2–H_2O solubility models (Newman and Lowenstern, 2002; Witham et al., 2012) to determine saturation pressures for melt inclusions in order to reconstruct the extent of CO_2 degassing as a function of pressure within the Laki magmatic system, and to assess how CO_2 degassing is coupled to melt mixing and fractional crystallisation for large basaltic fissure eruptions. Finally, we present an updated petrologic method for estimating the total atmospheric yield of CO_2 from magmas, which takes into account both the sequestration of CO_2 into vapour bubbles, and the diversity of parental melts supplied to the magmatic system. This method can be used to assess both the 'erupted' CO_2 budget associated with melt ascent from the magma chamber to the surface, and the mass of CO_2 released through deep, passive degassing in the magmatic system.

2. Sample collection and analytical methods

Fresh, glassy samples of magmatic tephra were obtained from proximal fall deposits around the Laki cone row by digging down

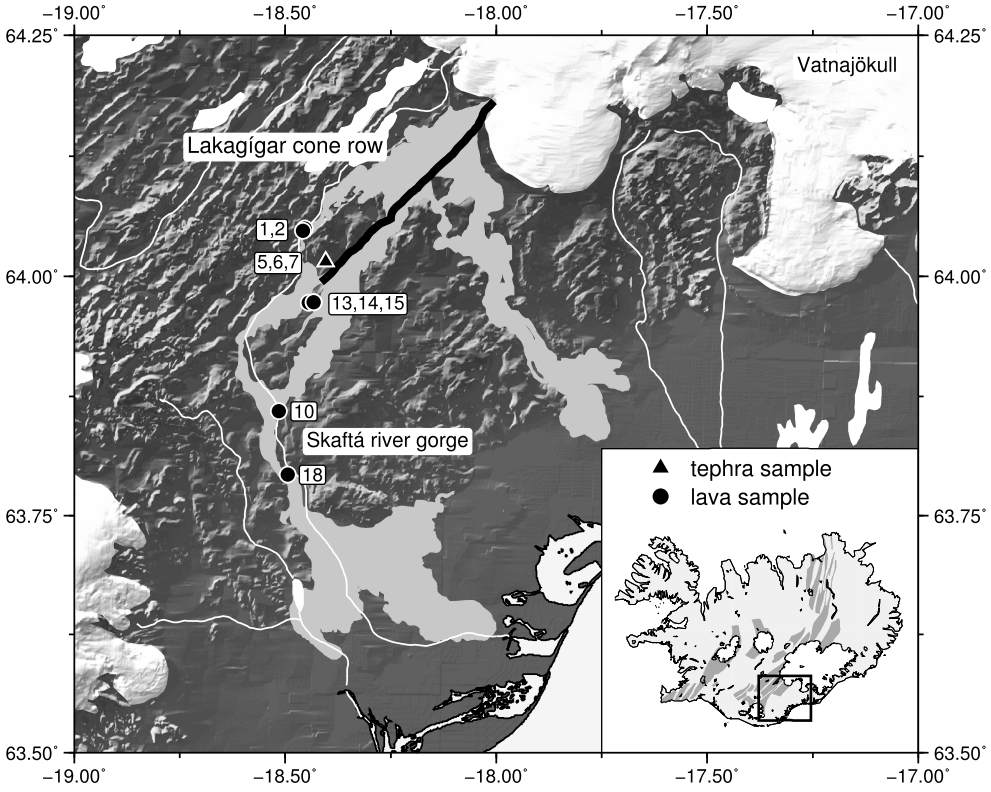

Fig. 1. Map of the Laki fissure and lava flow field within Iceland's Eastern Volcanic Zone (EVZ). Numbered locations show where the samples used in this study were collected. The inset map shows the location of the EVZ; fissure swarms are shaded in dark grey.

through the surface cover. Lava samples were collected from sites around the Skaftá river gorge, and samples were taken from glassy selvages on the upper and/or lower flow surfaces. Sample locations are shown in Fig. 1.

Olivine macrocrysts in the size range 250 μm to 1 mm were picked from crushed lava and tephra samples. Care was taken to select pale green, unaltered olivines containing glassy melt inclusions without post-entrapment daughter crystals, and with spherical to ellipsoidal shapes. Inclusion lengths and widths were measured from high resolution, high magnification photomicrographs using Zeiss AxioVision software; inclusions ranged from 5 to 450 μm in their longest dimension. Melt inclusion volumes were calculated assuming that inclusion depth was equal to the shorter of the measured dimensions. Vapour bubbles were present in 88% of the melt inclusions from lava samples and 41% of melt inclusions from tephra samples. Where present, the bubbles ranged from 1 to 78 μm in diameter. Of 937 bubble-bearing melt inclusions, 38 had bubbles comprising >5% of the melt inclusion volume. For the remaining 899 bubble-bearing melt inclusions, the bubble comprised on average1.5 ± 1.0 vol.% of the inclusion.

Olivines were mounted in CrystalBond and polished to expose a flat crystal surface, without breaching the melt inclusions. Compositions of vapour bubbles were then determined by micro-Raman spectroscopy, using the Horiba LabRam instrument at the University of Cambridge. The presence of CO_2 in fluid bubbles is verified by the presence of two characteristic peaks, at ∼1285 cm^{-1} and ∼1380 cm^{-1}, defining a Fermi diad in the Raman spectrum. Fermi diads can be observed in the micro-Raman spectra of bubbles down to 1 μm in diameter, so the success of the technique is not limited by bubble size. The Fermi diad spacing, Δ, is proportional to the fluid density. Several calibrations have been proposed for calculating the density of pure CO_2 fluid inclusions, and a brief review of different densimeters is provided in the supplementary material. In this study we used the densimeter of Kawakami et al. (2003). The positions of the Fermi bands were determined by fitting Gaussian curves to the Raman spectra using OriginLab software. The error in the peak fitting procedure was used to estimate the precision in Δ, which in turn constrains the precision of the densimeter. Precision in Δ of ±0.1 cm^{-1} corresponds to a precision in fluid density of ±0.02 g/cm^3 for inclusions of 1 μm, and can be better for larger inclusions (Kawakami et al., 2003). Average precision in Δ was 0.002 cm^{-1} for the Laki bubbles, and the corresponding error in fluid density is negligible.

Following the Raman analyses, crystals were individually polished to expose the melt inclusions at the surface, mounted in resin and re-polished. Volatiles CO_2, H_2O and trace and rare earth elements (REE) were analysed in 106 melt inclusions and 9 matrix glasses by secondary ion mass spectrometry (SIMS) on the Cameca ims-4f ion microprobe at the University of Edinburgh. CO_2 was measured first, with the instrument configured to a high mass resolution sufficient to resolve interference by $^{24}Mg^{2+}$ on the ^{12}C peak. Trace elements and H_2O were then measured with the mass spectrometer configured to a lower mass resolution. Precision and accuracy for CO_2 and H_2O were monitored by repeat analyses of a suite of basaltic glass standards with known compositions (Shishkina et al., 2010). Estimated 1σ precision and accuracy were ±5% and ±1% respectively for CO_2, and ±4% and ±2% respectively for H_2O. Precision and accuracy for the trace element measurements were monitored by repeat analyses of standards NIST-SRM610, BCR-2G and KL2-G. 1σ accuracy for the trace elements was estimated as ±10%. Precision was generally better than ±3% for trace elements in high abundance (e.g. Sr, Zr, La), and was ±8% for low-abundance heavy REEs. Major and minor element concentrations in the melt inclusions and their host olivines were measured by WDS Cameca SX100 electron microprobe (EPMA) at the University of Cambridge. Compositional data and details of all analytical methods are provided in the supplementary material.

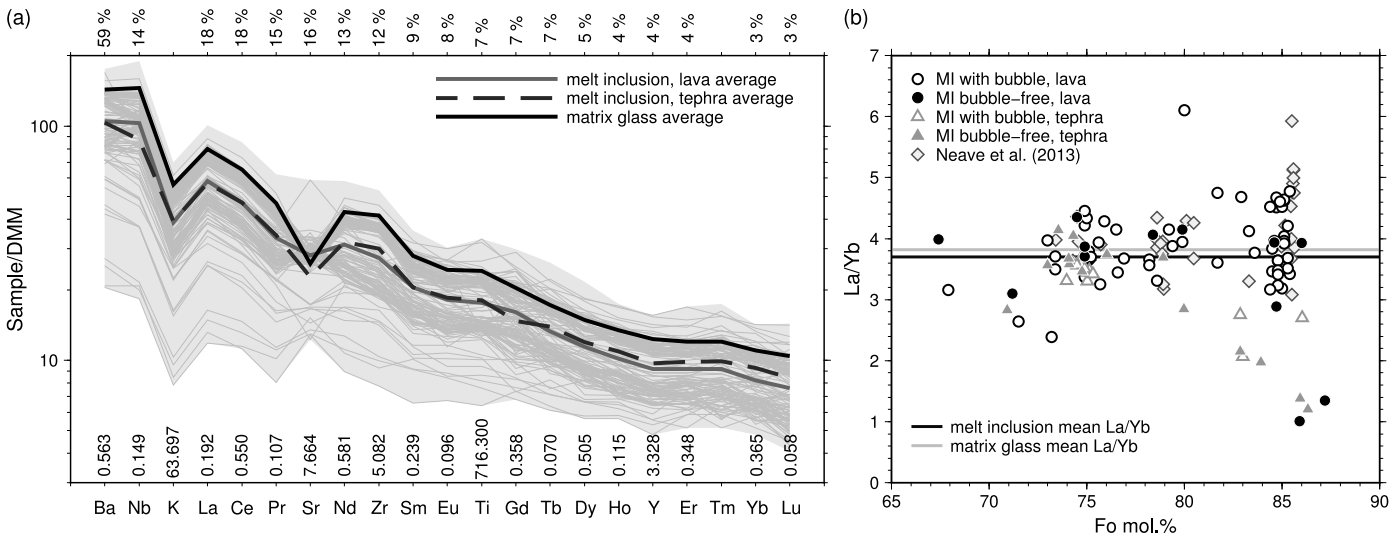

Fig. 2. (a) Multi-element diagram for Laki melt inclusions and matrix glasses. Concentrations normalised to depleted MORB mantle (DMM; Workman and Hart, 2005). Normalisation values are shown along the bottom of the plot; 2σ errors are shown along the top. The shaded area shows the range of melt inclusion and glass compositions. Individual melt inclusions are shown by the thin grey lines. Average compositions for melt inclusions in lava and tephra samples, and the matrix glass, are shown by the bold lines. (b) Host olivine forsterite content vs. La/Yb for Laki melt inclusions. Open symbols indicate bubble-bearing inclusions; closed symbols indicate bubble-free inclusions. Grey diamonds are data from Neave et al. (2013). The variability in La/Yb decreases with decreasing host forsterite content, which is interpreted as evidence of concurrent mixing and crystallisation of diverse mantle melt compositions within the Laki plumbing system (Neave et al., 2013). As crystallisation progresses, compositional diversity collapses to the mean melt inclusion value, shown by the black line. Similar behaviour is observed in samples from Borgarhraun, North Iceland, and across Iceland as a whole (Maclennan, 2008).

3. Results

3.1. Major elements

The melt inclusions range in composition from Mg# $\sim$ 62 to Mg# $\sim$ 30 (average Mg# = 47). Major element compositions of melt inclusions can be greatly affected by post-entrapment crystallisation (PEC), whereby continued crystallisation of olivine on the inclusion wall results in a drop in melt inclusion Mg# (e.g. Danyushevsky et al., 2000a). The extent of PEC experienced by each melt inclusion was estimated using Petrolog3 (Danyushevsky and Plechov, 2011). While some melt inclusions experienced PEC up to 7%, most inclusions experienced $\leqslant$2% PEC, and the PEC corrections are minor. Melt inclusion-bearing olivine macrocrysts range in composition from Fo_{86} to Fo_{67}. Olivines from lava samples were slightly more forsteritic with average compositions of $Fo_{80\pm5}$; olivines from tephra samples had average compositions of $Fo_{77\pm4}$. Assuming a $Kd^{ol\text{-}liq}_{Fe\text{-}Mg} = 0.31 \pm 0.03$ (Danyushevsky, 2001), the Laki carrier liquid composition is in equilibrium with Fo_{71}–Fo_{68} olivine.

3.2. Trace elements

Melt inclusions from lava and tephra samples have very similar average trace element concentrations, but have slightly lower average trace element abundances than the average matrix glass composition (Fig. 2a). The matrix glasses and many of the melt inclusions are depleted in Sr, which is indicative of plagioclase crystallisation from the melt prior to inclusion entrapment.

Matrix glasses have an average La/Yb of 3.8 ± 0.2 (1σ), while the melt inclusions have a mean La/Yb of 3.6 ± 0.8 (Fig. 2b). A single melt inclusion had a highly enriched composition with La/Yb of 6.1. Four inclusions have highly depleted compositions (La/Yb $\leqslant$ 1.5). These highly depleted melt inclusions were present in $Fo_{>82}$ olivines from tephra samples, while the most enriched inclusions (La/Yb $>$ 4.5) were exclusively present in lava samples. The reason for this distribution is unclear, and might not persist if more inclusions were measured. The full range of La/Yb variability is present in melt inclusions hosted in $Fo_{>84}$ olivines, and the variability in La/Yb decreases with decreasing host forsterite content. At low forsterite contents, the melt inclusion compositions cluster about the mean melt inclusion La/Yb (Fig. 2b).

3.3. Volatiles

3.3.1. CO_2 in bubbles

Fermi diads were observed in the Raman spectra of 52% of bubbles in melt inclusions from lava samples ($n = 817$) and 6% of bubbles in melt inclusions from tephra samples ($n = 124$) (Fig. 3). Fluid densities calculated for the Laki bubbles ranged from a minimum of 0.031 g/cm^3 to a maximum of 0.566 g/cm^3. Bubbles in lava samples had an average fluid density of 0.143 $\pm$ 0.050 g/cm^3; for tephra samples the average fluid density was 0.181 $\pm$ 0.063 g/cm^3.

The CO_2 content of the vapour bubbles in ppm, $[CO_2]_{vb}$, can be calculated using the mass ratio between bubble and glass in the host melt inclusion:

$$[CO_2]_{vb} = \left(\frac{M^{CO_2}_{vb}}{M_{gl}}\right) \times 10^6 \quad (1)$$

where the mass of glass within the melt inclusion, M_{gl}, is calculated as the glass volume multiplied by a melt density of 2750 kg/m^3 (Passmore et al., 2012). The mass of CO_2 contained within the bubble, $M^{CO_2}_{vb}$, is calculated from the bubble volume and the measured fluid density (Table 1). The principal source of error in the calculated CO_2 content of the bubble therefore lies in the measurement of the inclusion and bubble sizes. The least precise measurements are of the smallest bubble diameters in the range 2–5 μm, where the error may be as large as $\pm$10%. In the worst-case scenario, whereby all inclusion and bubble measurements have errors of $\pm$10%, the precision in the calculated CO_2 content of the bubble is approximately $\pm$20%. Larger inclusions and bubbles can be measured with much greater accuracy, and measurements that are precise to $\pm$2% correspond to errors of $\pm$4% in the calculated bubble CO_2 content.

Bubbles in melt inclusions from lava samples contained between 68 and 135 400 ppm CO_2; bubbles in melt inclusions from tephra samples contained between 1474 and 46 422 ppm CO_2.

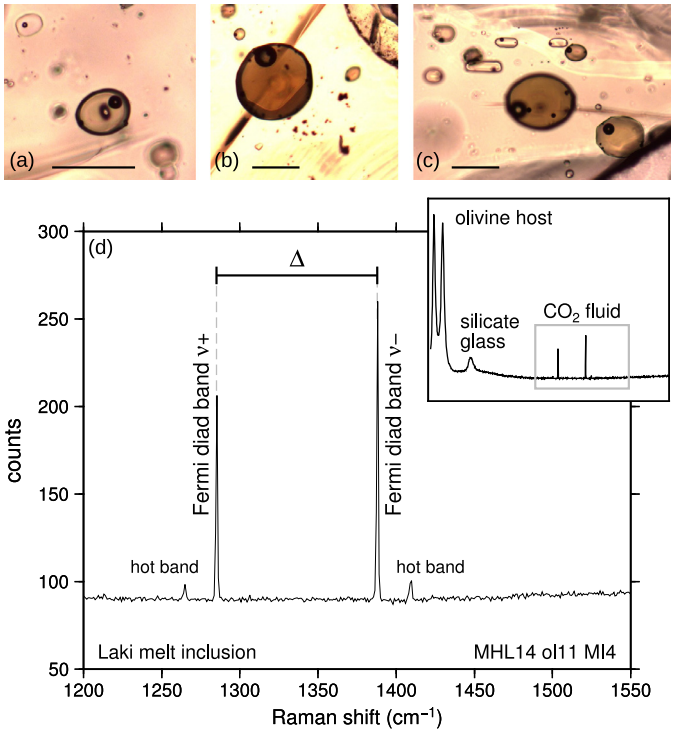

Fig. 3. (a) to (c): Plane-polarised light images of bubbles in olivine-hosted melt inclusions from Laki. The scale bar in each image is 100 μm. Where multiple melt inclusions are present within a single crystal, the bubbles occupy a similar volume fraction of their host inclusions. The bright area in the centre of the large melt inclusion in image (a) is a SIMS analysis spot. (d) Micro-Raman spectrum of a CO_2-bearing bubble in an olivine-hosted melt inclusion from Laki. The presence of CO_2 is confirmed by the Fermi diad, consisting of two peaks at 1285 and 1388 cm^{-1}, bounded by hot bands. The spacing of the Fermi diad, Δ, depends on the fluid density. The inset figure shows the location of the Fermi diad with respect to the Raman bands for olivine and silicate glass.

Eleven bubbles had CO_2 concentrations >6500 ppm, and all of these bubbles comprised >7% of their host melt inclusion's total volume. We assume that the Laki bubbles comprise pure CO_2 vapour, since no bands corresponding to H_2O, SO_2 or SO_4^{2-} were identified in any of the micro-Raman spectra. However, it is possible that additional volatile species are present in the bubbles in concentrations below the micro-Raman detection limits.

3.3.2. CO_2 and other volatiles in glass

Glass CO_2 concentrations in the melt inclusions range from 25 to 1433 ppm (Fig. 4a). The CO_2 concentration in the matrix glass was below the detection limit (<24 ppm) of the SIMS measurements. The average CO_2 concentration in melt inclusions from lava samples was 182 ppm, compared to 309 ppm for inclusions from tephra samples. Bubble-free melt inclusions contained on average 283 ± 236 ppm CO_2. For melt inclusions with CO_2-bearing vapour bubbles, the average CO_2 concentration in the glass was 151 ± 258 ppm. Inclusions with apparently CO_2-free bubbles contained 281 ± 256 ppm CO_2 in the glass.

Water concentrations in the melt inclusions range from 0.07 to 0.76 wt.%. Melt inclusions in lava samples contain an average 0.14 ± 0.13 wt.% H_2O, while inclusions from the tephra contain 0.55 ± 0.05 wt.% H_2O. Melt inclusions with CO_2-bearing bubbles contain 0.14 ± 0.13 wt.% H_2O. Bubble-free inclusions and those with CO_2-free bubbles contain 0.33 ± 0.23 and 0.31 ± 0.21 wt.% H_2O respectively. The matrix glass contains 0.08 ± 0.01 wt.% H_2O.

4. Discussion

4.1. Post-entrapment degassing: CO_2 sequestration into vapour bubbles

The micro-Raman spectra for vapour bubbles in melt inclusions from Laki lava samples showed the Fermi diad bands characteristic of CO_2. However, no Fermi diads were detected in the micro-Raman spectra for the majority of bubbles from tephra samples. This may indicate that CO_2 in these bubbles is present in concentrations below the detection limit of the instrument, which is better than 0.04 g/cm^2 CO_2, or that the bubbles contain no vapour and are a near-vacuum (e.g. Steele-MacInnis et al., 2011). The apparent absence of CO_2 from these bubbles may be related to the cooling rate, since CO_2 diffusion at the melt–gas interface is kinetically limited by the diffusivity of CO_2 in the melt (Pichavant et al., 2013), which is in turn dependent on temperature. Melt inclusions in the tephra were rapidly quenched upon eruption, and it is possible that the rapid cooling provided insufficient time for CO_2 to diffuse into shrinkage bubbles that formed in response to volume changes shortly before the inclusions passed through the glass transition. By contrast, melt inclusion-bearing olivines in the Laki lava spent hours to days in insulated transport before being quenched in the upper or lower selvages of lava flows. These melt inclusions cooled quickly enough to preserve glassy inclusions with no post-entrapment daughter crystals, but spent sufficient time in a hot environment at atmospheric pressure to permit CO_2 diffusion into shrinkage bubbles prior to solidification.

Glass CO_2 concentrations for bubble-bearing, CO_2-present; bubble-bearing, CO_2-free; and bubble-free inclusions are highly variable, and the datasets have standard deviations that are equal to or larger than the mean glass CO_2 contents. The Kolmogorov–Smirnov (KS) test was therefore used to examine whether the glass CO_2 contents for these three populations are significantly different. When comparing bubble-free melt inclusions with inclusions containing a CO_2-free bubble, the KS statistic (D) is 0.1304 and the p-value is 0.9897 at 95% confidence, indicating that there is no significant difference between these two populations. However, when comparing melt inclusions containing CO_2-bearing bubbles with bubble-free inclusions, the KS statistic is 0.587 and the p-value is 5.16×10^{-5}. There is therefore a significant difference in the glass CO_2 contents for these melt inclusion populations. These statistics demonstrate firstly that post-entrapment sequestration of CO_2 into the bubble is significant, but secondly that the presence of a vapour bubble is not necessarily indicative of CO_2 loss from the melt. It is only by analysing the bubble that the extent of CO_2 sequestration can be determined.

The total CO_2 concentration in bubble-free melt inclusions is simply the CO_2 concentration in the glass. The total CO_2 content of the bubble-bearing inclusions is the sum of CO_2 in the glass plus the CO_2 in the bubble (Fig. 4; Table 1). To ensure that this is representative of the melt CO_2 content at the time of inclusion entrapment, it is important to verify that the inclusion was trapped as a homogeneous liquid phase and that the bubbles formed by post-entrapment degassing. 'Pre-entrapment' bubbles, trapped as a vapour phase coexisting with the melt, may artificially skew the total inclusion CO_2 content to high values. True shrinkage bubbles formed by post-entrapment processes typically comprise 0.2–5 vol.% of an inclusion, with the actual value dependent on the initial volatile concentration, melt composition and cooling rate (Lowenstern, 1995, 2003). Visual inspection of olivines that host multiple melt inclusions reveals that, within a single crystal, bubbles occupy a similar volume fraction of each melt inclusion (Fig. 3a–c; Supplementary Fig. A), suggesting that the bubbles formed by a common post-entrapment process. Melt inclusions with unusually voluminous bubbles that may have been trapped as a vapour phase are easily recognisable,

Table 1
Calculation of total CO_2 contained within representative examples of melt inclusions from Laki.

	MHL01 ol13 MI2	MHL01 ol24 MI1	MHL05 ol4 MI1	MHL07 ol23 MI3	MHL06 ol23 MI3
	lava	*lava*	*tephra*	*tephra*	*tephra*
Micro-Raman					
Fermi diad $\nu+$ (cm^{-1})	1285.20	1284.64	1284.77	n.d.	–
Fermi diad $\nu-$ (cm^{-1})	1387.92	1387.46	1387.52	n.d.	–
Δ (cm^{-1})	102.72	102.83	102.75	n.d.	–
Bubble					
Fluid density[a] (g/cm^3)	0.109	0.147	0.120	n.d.	–
Bubble width/depth (cm)	3.70×10^{-2}	1.40×10^{-2}	1.31×10^{-2}	1.75×10^{-2}	0
Bubble length (cm)	3.87×10^{-2}	1.52×10^{-2}	1.37×10^{-2}	2.24×10^{-2}	0
Bubble volume (cm^3)	2.77×10^{-5}	1.57×10^{-6}	1.23×10^{-6}	3.60×10^{-6}	0
CO_2 mass (g)	3.01×10^{-6}	2.31×10^{-7}	1.48×10^{-7}	n.d.	0
Melt inclusion					
Inclusion width/depth (cm)	1.29×10^{-1}	3.79×10^{-2}	3.23×10^{-2}	8.60×10^{-2}	9.40×10^{-2}
Inclusion length (cm)	1.42×10^{-1}	7.53×10^{-2}	4.76×10^{-2}	1.17×10^{-1}	1.14×10^{-1}
Inclusion volume (cm^3)	1.23×10^{-3}	5.67×10^{-5}	2.60×10^{-5}	4.53×10^{-4}	5.26×10^{-4}
Glass					
Glass volume[b] (cm^3)	1.20×10^{-3}	5.51×10^{-5}	2.47×10^{-5}	4.49×10^{-4}	5.26×10^{-4}
Glass density (g/cm^3)	2.75	2.75	2.75	2.75	2.75
Glass mass (g)	3.382×10^{-3}	1.557×10^{-3}	7.127×10^{-5}	1.246×10^{-3}	1.445×10^{-3}
Inclusion mass[c] (g)	3.385×10^{-3}	1.559×10^{-3}	7.142×10^{-5}	1.246×10^{-3}	1.445×10^{-3}
Bubble (vol.%)	2.3	2.8	4.7	0.8	0
CO_2 *contents*					
CO_2 in glass[d] (ppm)	97	107	146	975	672
CO_2 in bubble (ppm)	892	1484	2076	$\geqslant$0	0
CO_2 in inclusion[e] (ppm)	989	1591	2222	$\geqslant$975	672
% CO_2 in bubble	90	93	93	$\geqslant$0	0

[a] Fluid density calculated using the equation of Kawakami et al. (2003).
[b] Glass volume = inclusion volume − bubble volume.
[c] Inclusion mass = glass mass + bubble mass.
[d] Glass CO_2 measured by SIMS.
[e] Total CO_2 in inclusion = glass CO_2 + bubble CO_2.

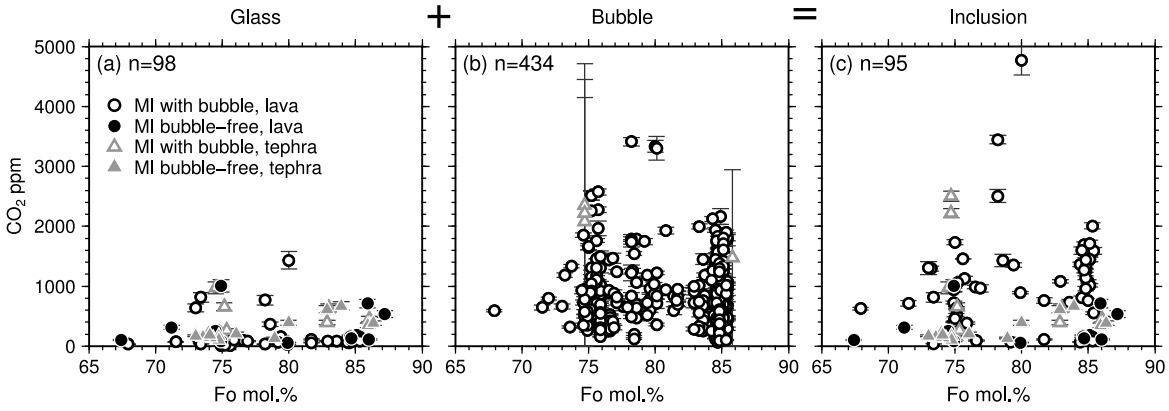

Fig. 4. CO_2 content of olivine-hosted melt inclusions from Laki. Open symbols indicate bubble-bearing inclusions; closed symbols indicate bubble-free inclusions. CO_2 concentrations in silicate glass were determined by SIMS; for bubble-free melt inclusions this represents the total CO_2 content. For bubble-bearing melt inclusions, the CO_2 content of the bubble was determined by micro-Raman spectroscopy; the total CO_2 in the inclusion is then the sum of the silicate glass and the bubble. For bubble-bearing inclusions, the total CO_2 concentration is greater than that of the silicate glass, which highlights the importance of post-entrapment degassing within melt inclusions. 2σ error bars are shown.

especially in crystals that host multiple melt inclusions (Supplementary Fig. B). In order to exclude such melt inclusions from further analysis, the Laki dataset was filtered to remove inclusions where bubbles comprised >5% of the total inclusion volume.

The available Raman and SIMS data enabled the total melt inclusion CO_2 to be calculated for 70 bubble-bearing and 25 bubble-free melt inclusions (Fig. 4c). Total CO_2 concentrations in the inclusions range from 384 to 4767 ppm, with an average of 1281 ± 781 ppm for melt inclusions with CO_2-bearing bubbles, 281 ± 256 ppm for inclusions with CO_2-free bubbles, and 283 ± 236 ppm for bubble-free inclusions. These results demonstrate that, for bubble-bearing melt inclusions, the total CO_2 contained in the inclusion can be significantly underestimated if CO_2 degassing into the vapour bubble is not taken into account (Fig. 4). CO_2 sequestration into bubbles appears to be enhanced for volatile-rich inclusions: the most CO_2-rich inclusions are most likely to form bubbles (Fig. 4c). The bubbles may comprise ⩽5 vol.% of the bubble-bearing melt inclusions, but they contain ∼90% of the total CO_2 in the Laki inclusions (Fig. 5). The percentage of CO_2 sequestered in the bubble is unrelated to the size of the melt inclusion and the composition of the host olivine, so these measurements cannot be used as proxies for CO_2 exsolution into the bubble.

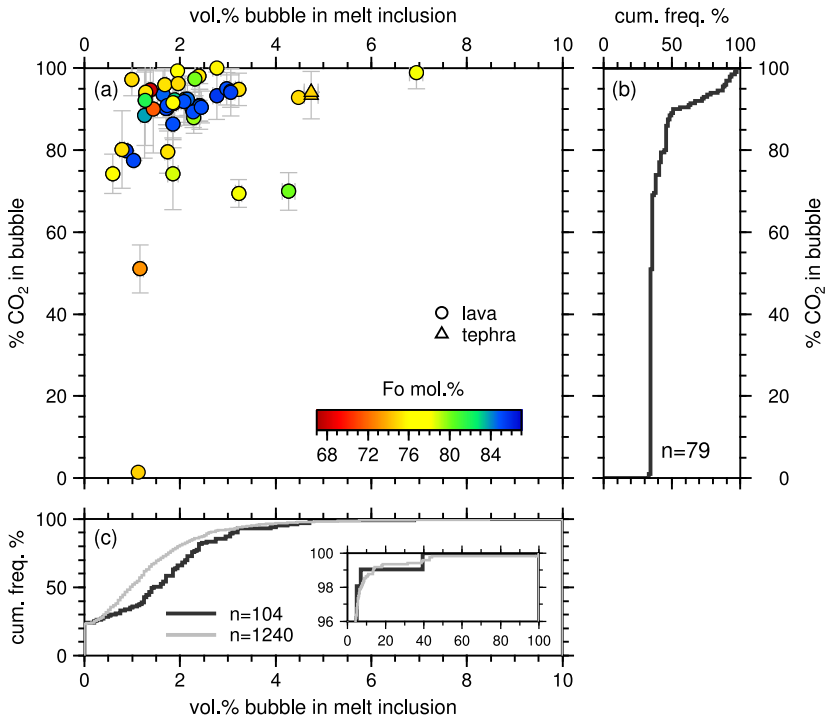

Fig. 5. (a) Relationship between bubble size and CO_2 sequestration into the bubble for olivine-hosted melt inclusions from Laki. There is no relationship between the proportion of the inclusion occupied by the bubble and the composition of the host olivine. (b) Cumulative frequency plot showing the percentage of CO_2 sequestered into the bubble for 79 bubble-bearing melt inclusions where CO_2 was measured in both the glass and the bubble. CO_2-free bubbles are present in 32% of these inclusions. For the CO_2-bearing bubbles, >90% of the total melt inclusion CO_2 may be sequestered into the bubble. (c) Cumulative frequency plot showing the volume percentage of the melt inclusion occupied by the bubble. The black line represents the 104 melt inclusions that were analysed by SIMS; the grey line represents the 1240 melt inclusions for which melt inclusion and bubble dimensions were measured. For 96% of bubble-bearing melt inclusions, the bubble comprises <5% of the total inclusion volume. The inset figure shows the size distribution of bubbles that comprise >5% of the total inclusion volume.

4.2. Melt inclusion saturation pressures

Saturation pressures for the melt inclusions, once the bubble CO_2 had been accounted for, were calculated using the CO_2–H_2O solubility models VolatileCalc (Newman and Lowenstern, 2002) and SolEx (Witham et al., 2012). The calculated saturation pressures are highly variable, ranging from 0.1 to >5 kbar for both lava and tephra samples (Fig. 6). If the glass CO_2 content is used for the saturation pressure calculations, all the Laki inclusions appear to have been trapped at pressures ⩽3 kbar. This demonstrates that if CO_2 in the bubble is not taken into account then saturation pressures for melt inclusions can be significantly underestimated.

Volatile solubility models assume equilibrium at the time of melt inclusion entrapment. Therefore, if an inclusion is trapped during crystallisation of a vapour-undersaturated melt, the calculated saturation pressure will underestimate the true entrapment pressure. Clinopyroxene-liquid thermobarometry suggests that the final stages of crystal-melt equilibration and growth of crystal rims occurred at pressures of 0.7–1.8 kbar (Neave et al., 2013). However, 16 of the bubble-free melt inclusions record much lower saturation pressures of 0.1–0.7 kbar (Fig. 6). Only two of these inclusions are hosted in Fo_{68}–Fo_{71} olivines that are in equilibrium with the Laki carrier liquid. This suggests that most of the low saturation pressures do not represent shallow, late-stage crystallisation of the Laki magma. A possible explanation is that these 16 inclusions were trapped during crystallisation of a vapour-undersaturated melt; however, their low CO_2/Nb values (3.8–17.6) indicate that they were trapped from a partially degassed melt rather than an undegassed melt. Alternatively, it is possible that CO_2 vapour has been lost during ascent through fractures in the crystal that have since re-annealed (e.g. Métrich and Wallace, 2008). The calculated saturation pressures thus provide a minimum estimate of the true entrapment pressure.

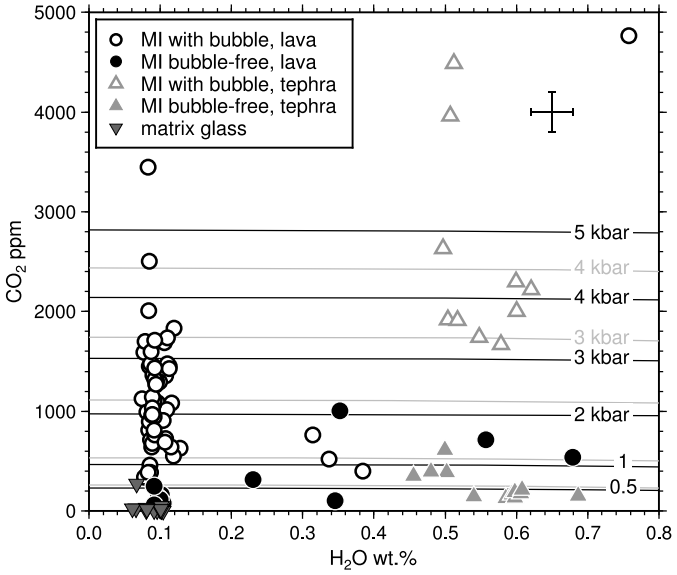

Fig. 6. H_2O and CO_2 contents of Laki melt inclusions. Open symbols indicate bubble-bearing inclusions; closed symbols indicate bubble-free inclusions. Isobars were calculated using VolatileCalc (black; Newman and Lowenstern, 2002) and SolEx (grey; Witham et al., 2012). At low H_2O concentrations, the isobars are strongly dependent on the CO_2 concentration. Melt inclusion saturation pressures calculated using the total inclusion CO_2 (glass + bubble) range from <0.1 to >5 kbar. Note that melt inclusions from lava samples have near-uniform H_2O concentrations of 0.1 wt.%, while inclusions from tephra samples contain 0.4–0.7 wt.% H_2O.

4.3. Diffusive H_2O re-equilibration and bubble formation

At magmatic temperatures, H^+ diffusion is capable of resetting the H_2O content of olivine-hosted melt inclusions in a matter

of hours to days (Gaetani et al., 2012; Bucholz et al., 2013). The near-uniform, low H_2O contents (~0.1 wt.% H_2O) in melt inclusions from Laki lava samples (Fig. 6) suggest that these inclusions have re-equilibrated with the Laki carrier liquid. By contrast, melt inclusions in the tephra preserve H_2O contents up to 0.69 wt.%, indicating that diffusive H^+ loss from these inclusions was much less extreme. The observation that melt inclusions in the tephra have only slightly modified H_2O contents suggests that diffusive re-equilibration of H_2O occurred primarily during insulated lava transport. There is no correlation between H_2O and Ce, which confirms the diffusive re-equilibration of H_2O in Laki lava samples.

Decompression associated with diffusive H^+ loss may facilitate the formation of bubbles in melt inclusions (Gaetani et al., 2012). It is therefore possible that post-entrapment degassing of CO_2 linked to H^+ diffusion may explain why the majority of melt inclusions in lava samples have vapour bubbles but the majority of inclusions from the tephra do not. However, there is no correlation between melt inclusion H_2O content and the proportion of the total CO_2 contained within the vapour bubbles (Supplementary Fig. C), which would be expected if CO_2 exsolution were driven by diffusive H^+ loss. The data therefore suggest that cooling and thermal contraction of the melt phase was the dominant control on bubble formation for the Laki melt inclusions, and that diffusive H^+ loss provided only a minor contribution to bubble growth.

4.4. Concurrent mixing, crystallisation and degassing in the Laki magma

The solubility of CO_2 in basaltic melt is strongly dependent on pressure and initial volatile content (e.g. Moore, 2008; Shishkina et al., 2010); therefore, CO_2 degassing is strongly controlled by the depths of magma storage and crystallisation. Solubility models (e.g. Dixon et al., 1995; Shishkina et al., 2010) can be used to predict the degassing path of basaltic magmas for different crystallisation models, and CO_2/Nb values can be used to deconvolve the effects of crystallisation and degassing.

For Icelandic basalts, it is likely that melts become saturated in a CO_2-rich vapour at depths of ~25 km (e.g. Pan et al., 1991; Dixon et al., 1995; Papale, 1999; Shishkina et al., 2010). If primary melts begin to crystallise at pressures higher than those required for vapour saturation, CO_2 will behave incompatibly, in a similar manner to Nb or Ba. Unless the melt is affected by mixing or contamination, CO_2/Nb will therefore remain constant until the melt becomes vapour-saturated at lower pressures and starts to degas. Olivines crystallising in the lower crust may thus trap inclusions from a CO_2-rich melt with a constant, high CO_2/Nb. Conversely, if primary melts ascend rapidly to a shallow level in the crust before crystallising, then CO_2 will degas prior to crystallisation and melt inclusions will typically be depleted in CO_2, with low CO_2/Nb. Where magma ascent, crystallisation and degassing occur concurrently in magmatic systems, CO_2/Nb should decrease steadily as crystallisation progresses and a broad positive correlation between CO_2/Nb and olivine composition is expected, although the correlation may not be linear. This is illustrated in Supplementary Fig. D. When coupled with indicators of the degree of melt fractionation and melt inclusion entrapment pressures, CO_2/Nb can be used to estimate (1) the expected CO_2 concentration of magmas stored in shallow reservoirs immediately prior to their eruption, and (2) the amount of CO_2 lost during passive degassing at lower- to mid-crustal pressures.

Melt inclusions from Laki record CO_2/Nb values that range from 3.8 to 364 (Fig. 7). Only one Laki melt inclusion has CO_2/Nb greater than the average CO_2/Nb of 314 ± 125 reported for Borgarhraun, North Iceland (Hauri et al., 2002). This high CO_2/Nb inclusion is the most enriched of the Laki inclusions (La/Yb = 6.1), and has a total CO_2 concentration of 4767 ppm and a calculated saturation pressure of 7.4 kbar. This inclusion may represent an undegassed melt, suggesting that the CO_2/Nb value of undegassed primary melts supplied to the Laki magmatic system lies towards the upper end of the Borgarhraun range, or may be even higher. The remaining Laki inclusions have CO_2/Nb < 262 and record saturation pressures <6 kbar, indicating that they were trapped during the crystallisation of partially degassed melts in the crust. Although the data are widely scattered, the average CO_2/Nb in the Laki inclusions decreases steadily with decreasing forsterite content of the host olivine (Fig. 7), indicating that degassing and crystallisation occurred concurrently within the magmatic system that eventually fed the Laki eruption. A similar trend is observed in CO_2/Ba (Supplementary Fig. E). All but one of the melt inclusions hosted in the most evolved ($Fo_{<75}$) olivines have CO_2/Nb values <100 and record saturation pressures <3.5 kbar. The latter stages of crystallisation of the Laki magma therefore occurred primarily in shallow magma reservoirs containing partially degassed magmas. The data also suggest that extensive fractionation of vapour-undersaturated melts in lower-crustal magma reservoirs was not significant in the Laki magmatic system over the crystallisation interval recorded by the $Fo_{<86}$ olivines.

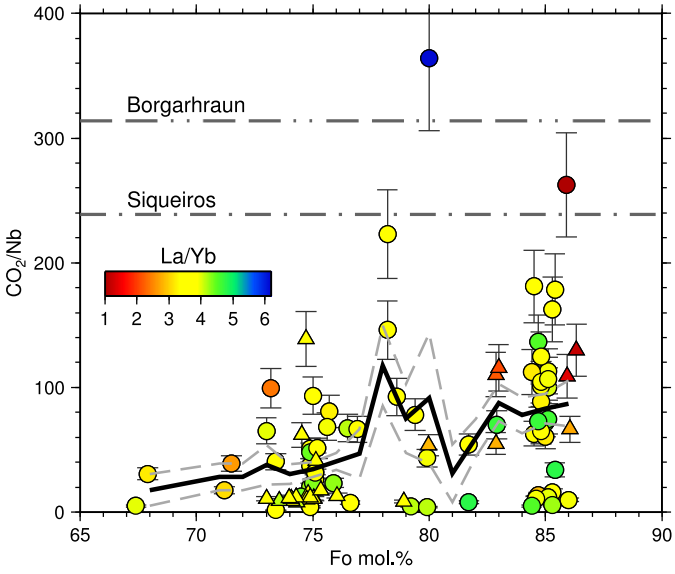

Fig. 7. (a) CO_2/Nb vs. host olivine composition for Laki melt inclusions, colour-coded for La/Yb. CO_2/Nb was calculated using the total inclusion CO_2 (glass + bubble), and showing the CO_2/Nb values determined from undegassed melt inclusions from Borgarhraun (314 ± 125; Hauri et al., 2002) and the Siqueiros transform fault (239 ± 46; Saal et al., 2002). 2σ error bars are shown. Black solid lines show the running average CO_2/Nb calculated using a boxcar filter with bandwidth of 2 mol.% Fo; grey dashed lines show the standard error of estimate (SEE) of the filtered data. The Laki melt inclusions appear to record concurrent degassing and crystallisation, with most melt inclusions being trapped during crystallisation of a partially or fully degassed magma.

4.5. Deep degassing path of the Laki magma

The predicted undegassed CO_2 content of each melt inclusion ($CO_2^{pr,mi}$) can be calculated from the measured Nb content of the melt inclusion (*mi*), if the CO_2/Nb of the initial primary melt (*ini*) is known:

$$CO_2^{pr,mi} = Nb^{mi}\left[\frac{CO_2}{Nb}\right]_{ini} \quad (2)$$

Undegassed CO_2 contents could be calculated using a single, fixed CO_2/Nb value, but this carries the assumption that the magma in question evolved by fractional crystallisation of a single primary melt with a given Nb content. This contrasts with recent studies of

melt inclusions from Icelandic eruptions, which have demonstrated that primary melts in Iceland are highly heterogeneous in their trace element and isotopic compositions (Maclennan et al., 2003; Maclennan, 2008). $Fo_{>84}$ olivines from Laki preserve melt inclusions with a wide range of La/Yb values (Fig. 2b), indicating that diverse enriched and depleted melt compositions were supplied to the Laki magmatic system (Neave et al., 2013). The variability in La/Yb decreases with decreasing host forsterite content (Fig. 2b), which is consistent with diverse primary melt compositions mixing and crystallising as they ascended through the crust, generating the homogeneous Laki carrier liquid composition erupted at the surface.

The wide range in CO_2/Nb (314 ± 125) determined for Borgarhraun (Hauri et al., 2002) may reflect the diversity of mantle melts supplied to Borgarhraun (Maclennan et al., 2003). It is expected that undegassed, enriched mantle melts with high Nb concentrations would also have high CO_2 concentrations, and a correspondingly greater CO_2/Nb than depleted primary melts (e.g. Michael and Graham, 2013). We therefore calculate the predicted CO_2 content of each melt inclusion using two methods: firstly with a fixed CO_2/Nb of 314, and secondly with CO_2/Nb = 435 for the enriched endmember and CO_2/Nb = 171 for the depleted endmember. CO_2/Nb values for the enriched and depleted endmembers were estimated from the few published studies of CO_2 and Nb concentrations in nominally undegassed melt inclusions (see Supplementary Fig. F for further details), and are close to the upper and lower bounds of the Borgarhraun value. The proportions of enriched and depleted endmembers and the extent of crystallisation required to generate the measured compositions of the Laki melt inclusions were calculated following the method of Maclennan (2008). The choice of CO_2/Nb values for the enriched and depleted endmembers is the major source of uncertainty in subsequent calculations.

Once the predicted undegassed CO_2 content of each melt inclusion has been calculated, the amount of CO_2 lost from each inclusion during degassing, $CO_2^{lost,mi}$, can be estimated by subtracting the amount of CO_2 measured in the inclusion, $CO_2^{meas,mi}$:

$$CO_2^{lost,mi} = CO_2^{pr,mi} - CO_2^{meas,mi} \tag{3}$$

This is shown in Fig. 8. It is important to note that, unless the CO_2 contained within vapour bubbles is taken into account, the CO_2 lost from the melt inclusions will be overestimated. Melt inclusions with the highest saturation pressures have lost the least CO_2 prior to entrapment (Fig. 8), as is predicted from solubility models. At any given pressure, the most enriched inclusions have lost the most CO_2, while the most depleted inclusions have lost almost none of their CO_2. This is observed whether a fixed or variable CO_2/Nb is assumed for the primary melt. Enriched primary melts, with higher absolute CO_2 concentrations than depleted primary melts, are most useful for investigating deep degassing in magmatic systems because a range of melt inclusion saturation pressures are recorded during crystallisation and degassing. Depleted melt inclusions with low initial CO_2 concentrations are not useful for constraining deep degassing behaviour, because they remain vapour-undersaturated to shallow levels.

4.6. Mass of CO_2 degassed from the Laki magma

The total mass of CO_2 lost from the Laki magma can be calculated by associating each inclusion with a mass of melt. The mass of melt present in the Laki magmatic system when a melt inclusion is trapped, M^{melt}, can be calculated as follows:

$$M^{melt} = \frac{(1 - X_{mi})}{(1 - X_{gl})} M^{tot} \tag{4}$$

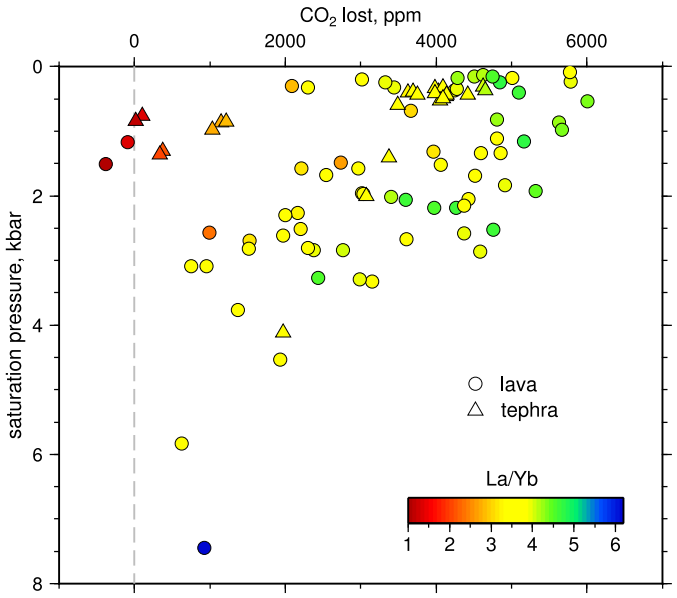

Fig. 8. Predicted CO_2 loss calculated for each melt inclusion; symbols colour-coded for La/Yb. Melt inclusions trapped at the highest pressures have lost the least CO_2 prior to entrapment, as is expected from solubility models. At any given saturation pressure, the most depleted inclusions have lost the least CO_2 since they remain vapour-undersaturated to very shallow levels. The most depleted melt inclusions, with La/Yb $\approx$ 1, appear to be undegassed.

where X_{mi} is the extent of crystallisation from the initial primary melt required to generate the melt inclusion composition, and X_{gl} is the extent of crystallisation required to produce the average matrix glass composition. The total mass of magma erupted from the Laki fissure, M^{tot}, was estimated assuming a total erupted volume of 15.1 km^3 (Thordarson and Self, 1993) and a melt density of 2750 kg/m^3 (Passmore et al., 2012). The mass of melt represented by each melt inclusion can then be calculated by taking a running or weighted mean of N inclusions:

$$M^{mi} = \frac{M^{tot}}{N} \frac{(1 - \overline{X_{mi}})}{(1 - X_{gl})} \tag{5}$$

The cumulative CO_2 lost is then given by:

$$M^{tot}_{CO_2} = \sum_{i=1}^{N} M^{mi,i} CO_2^{lost,mi,i} \tag{6}$$

The total CO_2 mass release for the Laki magma, $M^{tot}_{CO_2}$, was calculated using forward and inverse models. The inverse model used the Petrolog3 program (Danyushevsky and Plechov, 2011) to calculate a reverse fractional crystallisation trend for the Laki carrier liquid in 1% intervals, and the compositions of olivine, clinopyroxene and plagioclase in equilibrium with the melt were calculated at each interval. The value of $(1 - X_{mi})$ was then estimated for each melt inclusion by comparing its host olivine composition with the calculated reverse fractional crystallisation trend. This model assumes that the melt inclusions lie along a single liquid line of descent, and does not account for melt mixing in the Laki magmatic system. The forward model used the method of Maclennan (2008) to calculate the proportions of enriched and depleted endmembers, and the extent of fractional crystallisation required to generate each of the Laki melt inclusion compositions (X_{mi}) and the glass composition (X_{gl}). The enriched and depleted endmembers used in this calculation represent the most extreme compositions present in Icelandic melt inclusions.

The results of our calculations are summarised in Fig. 9. The preferred value of CO_2 mass release is 304 Mt, which was calculated using the inverse model with variable CO_2/Nb for enriched

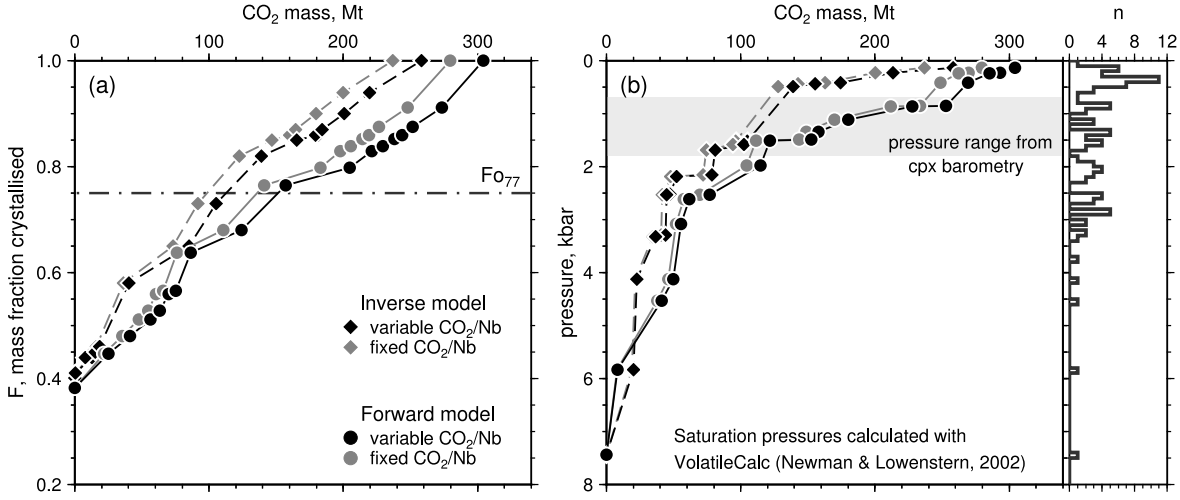

Fig. 9. Cumulative CO_2 mass release from the Laki magma. The inverse model was calculated by reverse fractional crystallisation of the Laki tephra glass composition (Danyushevsky and Plechov, 2011), and does not account for magma mixing in the Laki plumbing system. The forward model uses the method of Maclennan (2008) to calculate the effect of concurrent crystallisation and mixing of enriched and depleted parental melts. Approximately 300 Mt CO_2 was released from the Laki magma. The choice of fixed or variable CO_2/Nb for the magma source does not significantly affect the calculated total CO_2 mass release. (a) Cumulative CO_2 mass release vs. mass fraction crystallised, demonstrating that crystallisation and degassing occurred concurrently in the Laki magma. F = 1 is defined to be the composition of the Laki carrier liquid at the time of eruption, which is in equilibrium with Fo_{71}–Fo_{68} olivine. If the value of F associated with the composition of magma stored within the magma reservoir immediately prior to eruption is known, then it is possible to estimate the CO_2 release expected if that magma were to erupt. For example, if magma stored in the Laki magma chamber was in equilibrium with Fo_{77} olivine, corresponding to F = 0.75, then ~50% of the total CO_2 release would be associated with magma chamber degassing as this melt crystallised, ascended and erupted, i.e. melts where 0.75 < F < 1. The remaining ~50% of the CO_2 would then be associated with passive degassing from parental melts to those stored in the magma chamber, in equilibrium with Fo > 77 olivine (i.e. F < 0.75), as they fractionated in the lower crust. (b) Cumulative CO_2 mass release vs. melt inclusion saturation pressure. The histogram shows the number of analyses per 0.1 kbar pressure interval. Over 80% of the CO_2 mass release occurred in the shallow crust at pressures <3 kbar. The grey shaded region shows the pressures of final mineral-melt equilibration predicted using clinopyroxene-melt barometry (Neave et al., 2013). Melt inclusions recording saturation pressures shallower than this depth range may have undergone CO_2 loss, and their calculated saturation pressures provide a minimum estimate of the entrapment pressure.

and depleted endmember compositions. This is the only calculation to take into account the full extent of geochemical variability in the melts supplied to the Laki magmatic system. However, the calculations using fixed CO_2/Nb produce estimates of CO_2 mass release that are only 8% lower than if variable CO_2/Nb is used. The value of 304 Mt CO_2 refers to the total mass of CO_2 released from the Laki magma, and includes deep, 'passive' degassing as well as the CO_2 release associated with magma ascent during the eruption itself.

The rate of CO_2 degassing as a function of the mass fraction of melt crystallised is relatively constant (Fig. 9a). If the degree of fractionation required to generate the composition of magma stored within the magma reservoir immediately prior to eruption is known, it is possible to calculate both (1) the CO_2 release associated with the ascent and eruption of this magma composition, and (2) the CO_2 released passively as parental melts to those stored in the magma chamber fractionate in the lower crust. This is illustrated in Fig. 9a.

Our calculations suggest that approximately 60% of the total CO_2 mass release from Laki occurred at pressures ⩽2 kbar (Fig. 9b). This is similar to Kilauea volcano, Hawaii, where most of the CO_2 is exsolved at summit reservoir pressures between ~0.5 and 1 kbar (e.g. Gerlach, 1986; Gerlach et al., 2002). However, we note that melt inclusions recording saturation pressures <0.7 kbar may have been affected by CO_2 loss (see Section 4.2), and we suggest that these inclusions may have been trapped at pressures >1 kbar. The data may suggest that degassing from shallow magma storage zones dominated the Laki CO_2 budget. Alternatively, this shallow CO_2 release may be associated with the eruption itself, which would indicate that melt inclusions with shallow saturation pressures were trapped at a late stage, during magma ascent from a deeper crustal reservoir. Only ~16% of the CO_2 mass release at Laki occurred at pressures >4 kbar (Fig. 9b), which suggests that deep, passive CO_2 degassing formed only a minor contribution to the total CO_2 release from the Laki magmatic system.

Our calculated total mass release of 304 Mt CO_2 from the Laki magma is somewhat lower than the 348 Mt CO_2 calculated by Thordarson et al. (1996). There are several possible reasons for this discrepancy. Firstly, Thordarson et al. (1996) assumed pre-eruptive and 'degassed' CO_2 concentrations of 8530 and 1480 ppm respectively, which are almost certainly overestimates of the true CO_2 concentrations (Thordarson et al., 1996). This is an artefact of the analytical method, which measured the compositions of gases released by vacuum fusion of crushed melt inclusion-bearing plagioclase phenocrysts and of crushed tephra glass samples Óskarsson et al. (1984). Laki tephra glasses contain fluid-filled microbubbles (Ølafsson et al., 1984), and are therefore much more CO_2-rich than the true degassed Laki magma: our study indicates that glass from the Laki tephra has degassed almost all of its CO_2. Similarly, it has been suggested that Laki plagioclases contain CO_2 bubbles that were trapped as a free vapour phase during crystallisation (Métrich et al., 1991). It has also been demonstrated that the high-anorthite cores of Laki plagioclase macrocrysts did not crystallise directly from the Laki magma and are xenocrystic in origin (Neave et al., 2013); thus, any CO_2 contained in melt inclusions or bubbles in these high-anorthite cores cannot not be simply associated with the Laki magma. Secondly, our calculated CO_2 mass release of 304 Mt is based on a maximum CO_2/Nb of 435 for enriched Icelandic primary melts. If this value underestimates the true CO_2/Nb of enriched primary melts, then our calculations underestimate the initial CO_2 content of the Laki magma, and therefore provide only a minimum estimate of the total CO_2 mass release.

The values of CO_2 mass release calculated in this study and by Thordarson et al. (1996) are based on degassing from the mass of melt required to produce an erupted volume of 15.1 km^3 from the Laki vents, but do not account for CO_2 released from magma intruded into the shallow crust. If it is assumed that intrusions are emplaced at pressures of ~1–2 kbar, then these intrusions would be expected to degas between 40 and 60% of their total CO_2 (Fig. 9b). The ratio of erupted to intruded volume for the

Krafla Fires eruptions of 1975–1984 has been estimated at 0.3 (Harris et al., 2000). A similar erupted to intruded volume ratio for Laki would increase the total CO_2 mass release from Laki by 400–600 Mt, thus increasing the total CO_2 budget of the eruption by a factor of 2 to 3.

5. Conclusions

Volatile concentrations in olivine-hosted melt inclusions from Laki have been used to investigate post-entrapment degassing processes in melt inclusions and to reconstruct the deep degassing history of the Laki magma prior to its eruption. Vapour bubbles in melt inclusions from Laki may contain >90% of the total CO_2. This means that unless the CO_2 sequestration into bubbles is taken into account, the total CO_2 content of the inclusion will be underestimated, and any subsequently derived parameters such as saturation pressures calculated using solubility models will be too low. If post-eruption quenching is too rapid then CO_2 may not have sufficient time to diffuse into the bubble before solidification. The presence of a vapour bubble therefore cannot be taken as evidence that significant post-entrapment CO_2 exsolution has occurred within a melt inclusion.

The behaviour of CO_2 and Nb as similarly incompatible trace elements during crystallisation of a vapour-undersaturated melt enables the use of CO_2/Nb for deconvolving the effects of crystallisation and degassing. A positive correlation between CO_2/Nb and host olivine composition in the Laki melt inclusions demonstrates that crystallisation and degassing occurred concurrently in the Laki magmatic system. CO_2/Nb can also be used to reconstruct the undegassed CO_2 concentration of a melt inclusion if the CO_2/Nb of the primary melt is known. La/Yb variability in the Laki melt inclusions indicates that compositionally diverse mantle melts were supplied to the Laki magmatic system, and the enriched and depleted primary melts are expected to have different CO_2/Nb values. By modelling the combined effects of melt mixing, crystallisation and degassing, we have determined the degassing path of the Laki magma with respect to pressure and extent of crystallisation. Melt inclusions trapped at the highest pressures have lost the least CO_2, as predicted from volatile solubility models. At any given saturation pressure, the most enriched melt inclusions have lost the most CO_2, while depleted inclusions have degassed very little CO_2. Depleted melt inclusions with low CO_2 concentrations remain vapour-undersaturated to low pressures, and are therefore not useful for constraining deep degassing behaviour in magmatic systems.

We calculate that a minimum of 304 Mt CO_2 was released during degassing of the Laki magma. If CO_2 degassing from magma intruded into the upper crust is taken into account, the total CO_2 mass release from Laki may increase by 400–600 Mt, doubling or tripling the total CO_2 budget of the eruption. Our results demonstrate the utility of CO_2/Nb in investigating deep degassing processes, and have potential application for the development of gas flux monitoring at infrequently active basaltic volcanoes.

Acknowledgements

Support for this work was provided by NERC grants NE/I012508/1 and IMF-454/1011. We thank Richard Hinton at the Edinburgh Ion Microprobe Facility for his assistance during the ion probe analyses. Iris Buisman helped with the electron microprobe analyses. Issy Sides helped with the Raman spectroscopy measurements. This paper was improved by constructive discussions with David Neave, Issy Sides and Dan Morgan. We thank Alex Nichols, Andrey Gurenko and an anonymous reviewer for their thoughtful comments.

Appendix A. Supplementary material

Supplementary material related to this article can be found online at http://dx.doi.org/10.1016/j.epsl.2014.02.031.

References

Anderson, A.T., Brown, G.G., 1993. CO_2 contents and formation pressures of some Kilauean melt inclusions. Am. Mineral. 78, 794–803.
Bucholz, C.E., Gaetani, G.A., Behn, M.D., Shimizu, N., 2013. Post-entrapment modification of volatiles and oxygen fugacity in olivine-hosted melt inclusions. Earth Planet. Sci. Lett. 374, 145–155.
Carroll, M.R., Webster, J.D., 1994. Solubilities of sulfur, noble gases, nitrogen, chlorine and fluorine in magmas. Rev. Mineral. Geochem. 30, 231–279.
Cartigny, P., Pineau, F., Aubaud, C., Javoy, M., 2008. Towards a consistent mantle carbon flux estimate: Insights from volatile systematics (H_2O/Ce, δD, CO_2/Nb) in the North Atlantic mantle (14° N and 34° N). Earth Planet. Sci. Lett. 265, 672–685.
Cervantes, P., Kamenetsky, V., Wallace, P., 2002. Melt inclusion volatile contents, pressures of crystallization for Hawaiian picrites, and the problem of shrinkage bubbles. In: AGU Fall Meeting Abstracts, pp. V22A–V1217.
Chenet, A.L., Fluteau, F., Courtillot, V., 2005. Modelling massive sulphate aerosol pollution, following the large 1783 Laki basaltic eruption. Earth Planet. Sci. Lett. 236, 721–731.
Danyushevsky, L.V., 2001. The effect of small amounts of H_2O on crystallisation of mid-ocean ridge and backarc basin magmas. J. Volcanol. Geotherm. Res. 110, 265–280.
Danyushevsky, L.V., Plechov, P., 2011. Petrolog3: Integrated software for modeling crystallization processes. Geochem. Geophys. Geosyst. 12, 1–32.
Danyushevsky, L.V., Della-Pasqua, F.N., Sokolov, S., 2000a. Re-equilibration of melt inclusions trapped by magnesian olivine phenocrysts from subduction-related magmas: petrological implications. Contrib. Mineral. Petrol. 138, 68–83.
Danyushevsky, L.V., Eggins, S.M., Falloon, T.J., Christie, D.M., 2000b. H_2O abundance in depleted to moderately enriched mid-ocean ridge magmas; Part I: incompatible behaviour, implications for mantle storage, and origin of regional variations. J. Petrol. 41, 1329–1364.
Devine, J.D., Sigurdsson, H., Davis, A.N., Self, S., 1984. Estimates of sulfur and chlorine yield to the atmosphere from volcanic eruptions and potential climatic effects. J. Geophys. Res. 89, 6309–6325.
Dixon, J.E., 1997. Degassing of alkalic basalts. Am. Mineral. 82, 368–378.
Dixon, J.E., Clague, D.A., 2001. Volatiles in basaltic glasses from Loihi Seamount, Hawaii: Evidence for a relatively dry plume component. J. Petrol. 42, 627–654.
Dixon, J.E., Stolper, E.M., Holloway, J.R., 1995. An experimental study of water and carbon dioxide solubilities in mid-ocean ridge basaltic liquids. Part I: calibration and solubility models. J. Petrol. 36, 1607–1631.
Fischer, T.P., Marty, B., 2005. Volatile abundances in the sub-arc mantle: insights from volcanic and hydrothermal gas discharges. J. Volcanol. Geotherm. Res. 140, 205–216.
Gaetani, G.A., O'Leary, J.A., Shimizu, N., Bucholz, C.E., Newville, M., 2012. Rapid reequilibration of H_2O and oxygen fugacity in olivine-hosted melt inclusions. Geology 40, 915–918.
Gerlach, T.M., 1986. Exsolution of H_2O, CO_2, and S during eruptive episodes at Kilauea Volcano, Hawaii. J. Geophys. Res. 91, 12177–12185.
Gerlach, T.M., McGee, K.A., Elias, T., Sutton, A.J., Doukas, M.P., 2002. Carbon dioxide emission rate of Kilauea Volcano: Implications for primary magma and the summit reservoir. J. Geophys. Res. 107, ECV-3.
Hansteen, T.H., Klügel, A., 2008. Fluid inclusion thermobarometry as a tracer for magmatic processes. Rev. Mineral. Geochem. 69, 143–177.
Harris, A.J.L., Murray, J.B., Aries, S.E., Davies, M.A., Flynn, L.P., Wooster, M.J., Wright, R., Rothery, D.A., 2000. Effusion rate trends at Etna and Krafla and their implications for eruptive mechanisms. J. Volcanol. Geotherm. Res. 102, 237–270.
Hauri, E., Grönvold, K., Óskarsson, N., McKenzie, D., 2002. Abundance of carbon in the Icelandic mantle: constraints from melt inclusions. In: AGU Spring Meeting Abstracts, V51D-03.
Helo, C., Longpré, M.A., Shimizu, N., Clague, D.A., Stix, J., 2011. Explosive eruptions at mid-ocean ridges driven by CO_2-rich magmas. Nat. Geosci. 4, 260–263.
Kamenetsky, V.S., Davidson, P., Mernagh, T.P., Crawford, A.J., Gemmell, J.B., Portnyagin, M.V., Shinjo, R., 2002. Fluid bubbles in melt inclusions and pillow-rim glasses: high-temperature precursors to hydrothermal fluids?. Chem. Geol. 183, 349–364.
Kawakami, Y., Yamamoto, J., Kagi, H., 2003. Micro-Raman densimeter for CO_2 inclusions in mantle-derived minerals. Appl. Spectrosc. 57, 1333–1339.
Koleszar, A.M., Saal, A.E., Hauri, E.H., Nagle, A.N., Liang, Y., Kurz, M.D., 2009. The volatile contents of the Galapagos plume; evidence for H_2O and F open system behavior in melt inclusions. Earth Planet. Sci. Lett. 287, 442–452.
Lowenstern, J.B., 1995. Applications of silicate-melt inclusions to the study of magmatic volatiles. In: Thompson, J.F.H. (Ed.), Magmas, Fluids and Ore Deposits. In: Mineral. Assoc. Can. Short Course, vol. 23, pp. 71–99.

Lowenstern, J.B., 2003. Melt inclusions come of age: volatiles, volcanoes, and Sorby's legacy. Dev. Volcanol. 5, 1–21.
Maclennan, J., 2008. Concurrent mixing and cooling of melts under Iceland. J. Petrol. 49, 1931–1953.
Maclennan, J., McKenzie, D., Hilton, F., Grönvold, K., Shimizu, N., 2003. Geochemical variability in a single flow from northern Iceland. J. Geophys. Res. 108, 2007.
Métrich, N., Wallace, P.J., 2008. Volatile abundances in basaltic magmas and their degassing paths tracked by melt inclusions. Rev. Mineral. Geochem. 69, 363–402.
Métrich, N., Sigurdsson, H., Meyer, P.S., Devine, J.D., 1991. The 1782 Lakagigar eruption in Iceland – Geochemistry, CO_2 and sulfur degassing. Contrib. Mineral. Petrol. 107, 435–447.
Michael, P.J., 1995. Regionally distinctive sources of depleted MORB: Evidence from trace elements and H_2O. Earth Planet. Sci. Lett. 131, 301–320.
Michael, P.J., Graham, D.W., 2013. Concentration and behavior of CO_2 in MORB and OIB: a reevaluation. In: Goldschmidt2013 Conference Abstracts, p. 1752.
Moore, G., 2008. Interpreting H_2O and CO_2 contents in melt inclusions: constraints from solubility experiments and modeling. Rev. Mineral. Geochem. 69, 333–362.
Neave, D.A., Passmore, E., Maclennan, J., Fitton, G., Thordarson, T., 2013. Crystal–melt relationships and the record of deep mixing and crystallization in the AD 1783 Laki eruption, Iceland. J. Petrol. 54, 1661–1690.
Newman, S., Lowenstern, J.B., 2002. VolatileCalc: a silicate melt–H_2O–CO_2 solution model written in Visual Basic for excel. Comput. Geosci. 28, 597–604.
Nielsen, R.L., Michael, P.J., Sours-Page, R., 1998. Chemical and physical indicators of compromised melt inclusions. Geochim. Cosmochim. Acta 62, 831–839.
Ølafsson, M., Imsland, P., Larsen, G., 1984. Pele's hair II. Mode of formation, composition and structure. Náttúrufræðingurinn 53, 135–144.
Oman, L., Robock, A., Stenchikov, G.L., Thordarson, T., Koch, D., Shindell, D.T., Gao, C., 2006. Modeling the distribution of the volcanic aerosol cloud from the 1783–1784 Laki eruption. J. Geophys. Res. 111.
Óskarsson, N., Grönvold, K., Larsen, G., 1984. The haze produced by the Laki eruption. In: Einarsson, T., Gudbergsson, G.M., Gunnlaugsson, G.A., Rafnsson, S., Thorarinsson, S. (Eds.), Skaftáreldar 1783–1784: Ritgerdir og Heimildir. Mál og Menning, Reykjavík, pp. 67–80.
Palais, J.M., Sigurdsson, H., 1989. Petrologic evidence of volatile emissions from major historic and pre-historic volcanic eruptions. Geophys. Monogr. 52, 31–53.
Pan, V., Holloway, J.R., Hervig, R.L., 1991. The pressure and temperature dependence of carbon dioxide solubility in tholeiitic basalt melts. Geochim. Cosmochim. Acta 55, 1587–1595.
Papale, P., 1999. Modeling of the solubility of a two-component $H_2O + CO_2$ fluid in silicate liquids. Am. Mineral. 84, 477–492.
Passmore, E., Maclennan, J., Fitton, G., Thordarson, T., 2012. Mush disaggregation in basaltic magma chambers: evidence from the AD 1783 Laki eruption. J. Petrol. 53, 2593–2623.
Pichavant, M., Di Carlo, I., Rotolo, S.G., Scaillet, B., Burgisser, A., Le Gall, N., Martel, C., 2013. Generation of CO_2-rich melts during basalt magma ascent and degassing. Contrib. Mineral. Petrol. 166, 545–561.
Roedder, P.L., 1979. Origin and significance of magmatic inclusions. Bull. Minéral. 102, 487–510.
Saal, A.E., Hauri, E.H., Langmuir, C.H., Perfit, M.R., 2002. Vapour undersaturation in primitive mid-ocean-ridge basalt and the volatile content of Earth's upper mantle. Nature 419, 451–455.
Schiano, P., 2003. Primitive mantle magmas recorded as silicate melt inclusions in igneous minerals. Earth-Sci. Rev. 63, 121–144.
Schilling, J.G., Bergeron, M.B., Evans, R., Smith, J.V., 1980. Halogens in the mantle beneath the North Atlantic [and discussion]. Philos. Trans. R. Soc. Lond. Ser. A 297, 147–178.
Schmidt, A., Carslaw, K.S., Mann, G.W., Wilson, M., Breider, T.J., Pickering, S.J., Thordarson, T., 2010. The impact of the 1783–1784 AD Laki eruption on global aerosol formation processes and cloud condensation nuclei. Atmos. Chem. Phys. 10, 6025–6041.
Schmidt, A., Thordarson, T., Oman, D., Robock, A., Self, S., 2012. Climatic impact of the long-lasting 1783 Laki eruption: Inapplicability of mass-independent sulfur isotopic composition measurements. J. Geophys. Res. 117.
Shaw, A.M., Behn, M.D., Humphris, S.E., Sohn, R.A., Gregg, P.M., 2010. Deep pooling of low degree melts and volatile fluxes at the 85° E segment of the Gakkel Ridge: Evidence from olivine-hosted melt inclusions and glasses. Earth Planet. Sci. Lett. 289, 311–322.
Shishkina, T.A., Botcharnikov, R.E., Holtz, F., Almeev, R.R., Portnyagin, M.V., 2010. Solubility of H_2O- and CO_2-bearing fluids in tholeiitic basalts at pressures up to 500 MPa. Chem. Geol. 277, 115–125.
Sigurdsson, H., 1990. Assessment of the atmospheric impact of volcanic eruptions. In: Sharpton, V.L., Ward, P.D. (Eds.), Global Catastrophes in Earth History. In: Spec. Pap., Geol. Soc. Am., vol. 247, pp. 99–110.
Sigurdsson, H., Devine, J.D., Davis, A.N., 1985. The petrologic estimation of volcanic degassing. Jökull 35, 1–8.
Skirius, C.M., Peterson, J.W., Anderson Jr., A.T., 1990. Homogenizing rhyolitic glass inclusions from the Bishop Tuff. Am. Mineral. 75, 1381–1398.
Steele-MacInnis, M., Esposito, R., Bodnar, R.J., 2011. Thermodynamic model for the effect of post-entrapment crystallization on the H_2O–CO_2 systematics of vapor-saturated, silicate melt inclusions. J. Petrol. 52, 2461–2482.
Thomas, R., Kamenetsky, V.S., Davidson, P., 2006. Laser Raman spectroscopic measurements of water in unexposed glass inclusions. Am. Mineral. 91, 467–470.
Thordarson, T., Self, S., 1993. The Laki (Skaftár Fires) and Grímsvötn eruptions in 1783–1785. Bull. Volcanol. 55, 233–263.
Thordarson, T., Self, S., 2003. Atmospheric and environmental effects of the 1783–1784 Laki eruption: a review and reassessment. J. Geophys. Res. 108, 4011.
Thordarson, T., Self, S., Óskarsson, N., Hulsebosch, T., 1996. Sulfur, chlorine, and fluorine degassing and atmospheric loading by the 1783–1784 AD Laki (Skaftár fires) eruption in Iceland. Bull. Volcanol. 58, 205–225.
Thordarson, T., Self, S., Miller, D.J., Larsen, G., Vilmundardóttir, E.G., 2003. Sulphur release from flood lava eruptions in the Veiðivötn, Grímsvötn and Katla volcanic systems, Iceland. Geol. Soc. (Lond.) Spec. Publ. 213, 103–121.
Wallace, P., Carmichael, I.S.E., 1992. Sulfur in basaltic magmas. Geochim. Cosmochim. Acta 56, 1863–1874.
Webster, J., Kinzler, R., Mathez, E., 1999. Chloride and water solubility in basalt and andesite melts and implications for magmatic degassing. Geochim. Cosmochim. Acta 63, 729–738.
Witham, F., Blundy, J., Kohn, S.C., Lesne, P., Dixon, J., Churakov, S.V., Botcharnikov, R., 2012. SolEx: A model for mixed COHSCl-volatile solubilities and exsolved gas compositions in basalt. Comput. Geosci. 45, 87–97.
Workman, R.K., Hart, S.R., 2005. Major and trace element composition of the depleted MORB mantle (DMM). Earth Planet. Sci. Lett. 231, 53–72.
Workman, R.K., Hauri, E., Hart, S.R., Wang, J., Blusztajn, J., 2006. Volatile and trace elements in basaltic glasses from Samoa: Implications for water distribution in the mantle. Earth Planet. Sci. Lett. 241, 932–951.